energy&fuels

Article

pubs.acs.org/EF

Oxygen-Blown Entrained Flow Gasification of Biomass: Impact of Fuel Parameters and Oxygen Stoichiometric Ratio

Michael Kremling,*[,†] Ludwig Briesemeister,[†] Matthias Gaderer,[‡] Sebastian Fendt,[†] and Hartmut Spliethoff[†,§]

[†]Institute for Energy Systems, Technical University of Munich, Boltzmannstr. 15, 85748 Garching, Germany

[‡]Regenerative Energy Systems, Technical University of Munich, Schulgasse 16, 94315 Straubing, Germany

[§]ZAE Bayern, Walther-Meißner-Straße 6, 85748 Garching, Germany

ABSTRACT: Due to the high conversion rates and the low tar amounts in the product gas, entrained flow gasification of biomass can be an alternative process to state of the art gasification technologies, e.g., fluidized-bed gasifiers. Feedstock treatment is mandatory for entrained flow gasification (EFG). However, it has the potential of making residuals available for energetic use. In this study, the feasibility of EFG of solid biomass in an industrial-like test rig with a state of the art pneumatic dense-phase coal feeding system is shown. Four biomasses—torrefied wood (TW), beech wood (B), hydrothermal carbonized green waste (HCG), and corn cobs (CoC)—were used and compared to Rhenish lignite (RL). Especially, the gasification behavior of hydrothermal carbonized biomass is rarely known from the literature. The study includes a comparison of the fuels regarding feeding behavior, conversion rate, achievable gas composition, and cold gas efficiency (CGE) as well as tar formation. The oxygen stoichiometric ratio λ was varied from 0.35 to 0.55. Investigations have shown that B is not appropriate for the stable, long-term operation of a pneumatic dense-phase feeding system. B and CoC exhibited higher conversion rates at low λ values due to their higher volatile matter compared to the other fuels. The highest CGE of all trials was achieved with CoC (66.3%). B, CoC, and TW exhibited high amounts of CH_4 in the product gas, even at high temperatures. With regard to fuel conversion, HCG and TW generally behaved more like RL. Although EFG is often referred to be a tar-free technology, tar formation—investigated by solid-phase adsorption—was observed for all fuels especially at low λ values. Due to the high temperatures, mainly tertiary tars (e.g., naphthalene) were detected. A significant higher amount of tar was observed only for B (3.5 g/m^3). For all of the other fuels, the total amount of tar was <1 g/m^3 in all of the trials. Regarding feeding behavior, conversion rates and gas composition TW and HCG seem to be suitable as substitutes in coal fed gasification plants.

1. INTRODUCTION

The European Commission intends to reduce greenhouse gas emissions by 80−95% compared to 1990 levels.[1] Moreover, as outlined in the Paris Agreement, the international community has confirmed an overall goal to limit global warming to less than 2 °C in comparison to preindustrial times.[2] As a result, the energy supply—power generation as well as the supply of secondary energy carriers such as gasoline—has to be based on sustainable and renewable resources in the future. Energy from biomasses plays an important role in achieving this goal since its production is almost free of CO_2. Together with carbon capture and storage technology, it can even result in negative emissions. Furthermore, it is storable—in contrast to renewable energies from wind and sun.

The advantage of biomass gasification instead of a direct combustion is that several different utilization pathways are possible. For the generation of power, the efficiency of available conversion technologies is higher.[3] The state of the art in biomass gasification is fixed-bed and fluidized-bed gasifiers (FBG).[4−6] Due to their low operation temperatures, the produced gas contains a relatively high amount of tars, which requires an extensive treatment. In contrast, entrained flow gasification (EFG) is considered as a tar-free technology with high conversion rates and is state of the art in coal gasification plants.[7] The EFG of biomass is not a prevalent technology mainly because a homogeneous fuel with a high energy density is needed. This can be achieved by using fuel powders with small particle sizes or liquid fuels. Hence, for EFG, a pretreatment of the biomass is mandatory. However, it has already been proven theoretically that EFG of biomass can be competitive with FBG.[8,9] Experimental investigations of EFG of biomass have been published, e.g., by the Energy Technology Center in Sweden,[10−13] the Energy Research Center of The Netherlands (ECN),[14,15] and Qin et al.[16,17]

2. FUNDAMENTALS

2.1. Biomass Pretreatment for EFG. For state of the art EFG fed by pneumatic dense-phase conveying systems, the particle size of the fuel has to be <250 μm.[7,18] Woody biomasses can be milled to reach the required particle size. The electrical power consumption for milling wood to such small particle sizes is very high (up to 20% of the primary energy) and has a significant influence on the overall plant efficiency. Furthermore, the fiber-like structure of the particles leads to high cohesion forces between the particles causing problems with regard to fluidization characteristics and the application of pneumatic dense-phase conveying.[14]

Received: November 8, 2016
Revised: January 24, 2017
Published: February 22, 2017

DOI: 10.1021/acs.energyfuels.6b02949
Energy Fuels XXXX, XXX, XXX−XXX

Torrefaction (TF) is a thermal process in which a biomass is heated up to 200−300 °C under atmospheric pressure but in the absence of oxygen.[19] By using TF as a pretreatment, the energy consumption for milling is significantly lower compared to that required for thermally untreated biomasses (up to 90%).[8,15,20−24] In addition, the fluidization of the powder is easier. Not only the physical but also the chemical properties of the biomass are changed. Hemicellulose is decomposed. Cellulose is depolymerized, and lignin is thermally softened.[25]

Another pretreatment technology for biomasses is hydrothermal carbonization (HTC). The feedstock is treated in hot water at 175−250 °C and above the saturation pressure.[26] During the process, decarboxylation, dehydration, hydrolysis, condensation, and aromatization reactions take place.[27] After drying, the solid product can easily be grinded.[28] Since HTC as well as TF removes O_2 from the biomass, the heating value increases.

Thermal pretreatment processes lead to additional losses, which affect the total process chain efficiency. For TF, the energy yield (in relation to the original biomass) is in the range of 76−96%,[20] for HTC up to 89%.[28] ECN compared different process chains to generate a synthesis gas (40 bar) from raw biomass by EFG. Milling the biomass after drying to a particle size of 100 μm leads to an overall efficiency of 59%; milling to a particle size of 1 mm leads to 84%. The option with TF prior to pulverization shows 75%. However, the way with TF could be reasonable since existing feeding systems can be used and, due to the small particle size after TF and milling, a high fuel conversion is achieveable.[15] This concept is planned to be commercially realized in the BioTFuel project in the north of France until 2020.[29] Due to the wet process conditions during HTC, it is reasonable to carry out the process with wet and inhomogeneous biomasses and residuals such as green cut, spent grains, or sewage sludge. Therefore, the HTC process makes low-order biomass and waste streams accessible for power or fuel generation and produces a coal substitute.

2.2. EFG of Solid Biomass. The particle residence time during EFG is in the range of a few seconds. The temperatures reach up to 1600 °C.[7,18,30] The gasification agent is usually pure oxygen. The product is a high quality gas consisting mainly of CO and H_2. It can be converted to chemicals (e.g., ammonia, methanol), liquid and gaseous fuels (e.g., gasoline, SNG), or power (e.g., gas turbine).[7] EFG can be carried out in a slagging mode—the temperature is above the ash flow temperature—or in a nonslagging mode—the temperature is below the ash softening temperature. Using air instead of oxygen is possible, but this leads to lower temperatures and a product gas highly diluted with nitrogen. Conversion to chemicals is not possible in the case of air gasification. EFG is the preferred gasifier type for the gasification of coal and is usually operated at 20−70 bar.

When the fuel enters the EFG, it is heated up very quickly. The main reaction steps inside the gasifier are devolatilization, combustion of the char (1, 2) and the volatiles (3−5) with oxygen, followed by gasification of the char (6−8).[7,18,31−34] Devolatilization is completed within 10−200 ms.[35] The energy needed for the endothermic gasification reactions is provided by the combustion reactions. Assuming a complete carbon conversion, the reaction system can be reduced to homogeneous gas phase (reactions 9 and 10). At temperatures commonly reached in an EFG (>1200 °C), the equilibrium of reaction 10 is completely on the left-hand side.[7] In this case, the equilibrium of the gas phase can be described using only reaction 9 in good approximation.

For complete conversion, the only solid residue is either ash or slag (depending on whether the EFG is operated in a slagging or nonslagging mode).

Combustion reactions:

$$C + O_2 \rightarrow CO_2 \quad \Delta_R H^\circ = -393.5\ \text{kJ/mol} \tag{1}$$

$$C + 0.5O_2 \rightarrow CO \quad \Delta_R H^\circ = -110.5\ \text{kJ/mol} \tag{2}$$

$$CO + 0.5O_2 \rightarrow CO_2 \quad \Delta_R H^\circ = -283.0\text{kJ/mol} \tag{3}$$

$$H_2 + 0.5O_2 \rightarrow H_2O \quad \Delta_R H^\circ = -241.8\ \text{kJ/mol} \tag{4}$$

$$CH_4 + 2O_2 \rightarrow CO_2 + 2H_2O \quad \Delta_R H^\circ = -802.3\ \text{kJ/mol} \tag{5}$$

Char gasification reactions:

$$C + CO_2 \Leftrightarrow CO \quad \Delta_R H^\circ = +172.4.\ \text{kJ/mol} \tag{6}$$

$$C + H_2O \Leftrightarrow CO + H_2 \quad \Delta_R H^\circ = +131.3\ \text{kJ/mol} \tag{7}$$

$$C + 2H_2 \Leftrightarrow CH_4 \quad \Delta_R H^\circ = -74.9\ \text{kJ/mol} \tag{8}$$

Homogenous gas phase reactions:

$$CO + H_2O \Leftrightarrow CO + 3H_2 \quad \Delta_R H^\circ = -41.1\ \text{kJ/mol} \tag{9}$$

$$CO + 3H_2 \Leftrightarrow CH_4 + H_2O \quad \Delta_R H^\circ = -206.2\ \text{kJ/mol} \tag{10}$$

Generally, tars are defined as organic compounds that condense at room temperature.[6] According to DIN CEN/TS 15439, all hydrocarbons except C_1 to C_6 hydrocarbons fall under this definition.[36] In the presented study, tars are defined appropriate to the measurement range of the used tar sampling method. This definition includes all hydrocarbons with a molar mass higher than benzene (M = 78.11 g/mol) up to fluoranthene (252.31 g/mol). Tars originate from devolatilization when the macromolecules of the biomass are destroyed and gaseous compounds are formed.[37] Yu et al.[38] investigated tar formation from cellulose, hemicellulose, and lignin in an electrically heated entrained flow reactor and concluded that tars formed during lignin gasification are more stable and harmful than tars from cellulose and hemicellulose. Evans and Milne[39] classify tars according to their formation during heating up into three groups. Initially, primary tars such as furfural are released. With increasing temperatures, the tar composition changes, and secondary tars such as phenols or alkenes are formed. At temperatures above 800 °C, only tertiary tars (aromatics such as benzene, naphthalene, and toluene) remain. They are formed by the recombination of fragments of primary and secondary tars. The widely used ECN classification categorizes tars into five groups according to their size and the number of rings.[40,41]

The amount of tar in the product gas depends on the type of gasifier used: circulating FBG produces 2−30 g/m^3; updraft fixed-bed gasifiers, 10−150 g/m^3; and downdraft fixed-bed gasifiers, 0.1−6 g/m^3.[3] Depending on the syngas utilization, the tar amount has to be reduced. For example, for a gas engine or fuel cell, <100 mg/m^3 is allowed. Gas turbines require <5 mg/m^3, whereas synthesis processes can only handle <0.1 mg/m^3.[3,6] Besides the total tar amount, the tar dew point is another characteristic value. For its estimation, the concentration of every single tar compound is needed.[41] Especially for downstream processes where the product gas is used at low

DOI: 10.1021/acs.energyfuels.6b02949
Energy Fuels XXXX, XXX, XXX−XXX

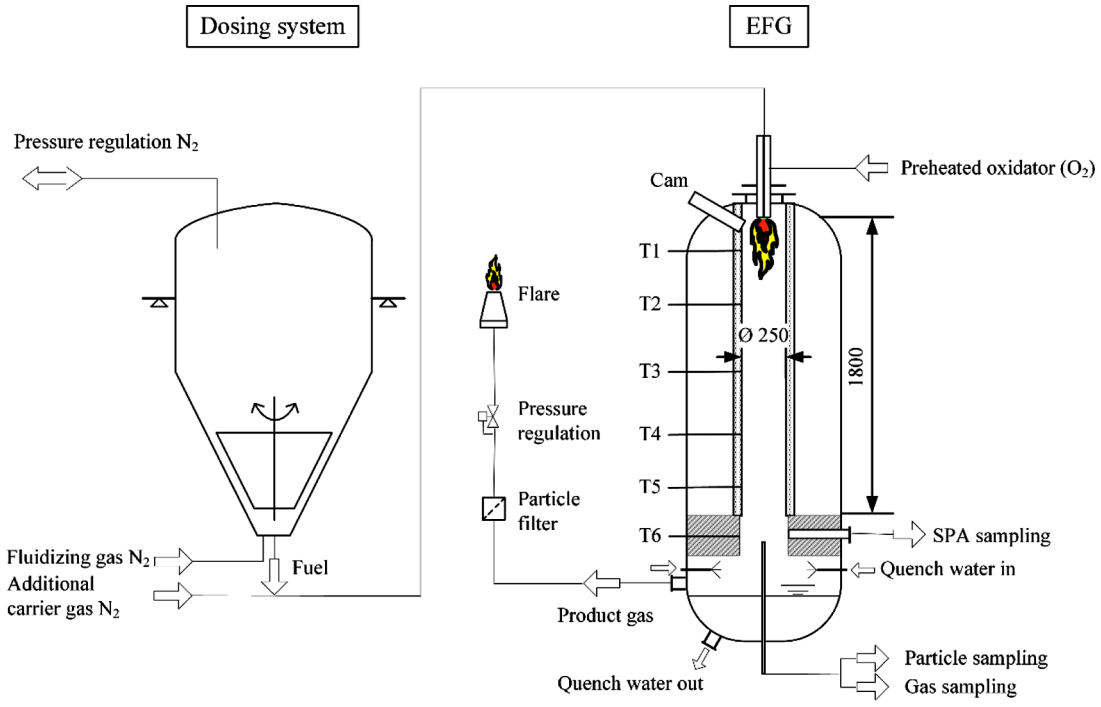

Figure 1. Simplified scheme of the BOOSTER test rig.

temperatures, it is necessary to know the tar dew point and to keep the temperature well above this dew point. If this is not possible, the tar must be removed from the product gas.

EFG is often considered to be a tar-free gasifier, although systematic investigations of the tar content and the composition of oxygen-blown entrained flow biomass gasification are not known to the authors. This work will contribute to close this knowledge gap.

In the present work, the feasibility of the EFG of biomasses in an industrial-like test rig is illustrated and compared with the results achieved with Rhenish lignite (RL). A solid feeding with a state of the art pneumatic dense-phase coal feeding system is considered to be an alternative to liquid feeding. Applied pretreatment methods are TF, HTC, and milling. The gasification of HTC biomasses in an autothermally operated EFG using O_2 is not yet known to the authors. The focus lies on the achievable gas composition and quality (including tar amount and tar composition) using different fuels and varying the oxygen stoichiometric ratio as the main process parameter.

3. EXPERIMENTAL SECTION

3.1. BOOSTER Test Rig. The BOOSTER (BiOmass pilOt-Scale enTrained flow gasifiER) test rig consists of two main components: the dosing system and the EFG (Figure 1). It is designed for operating pressures of up to 5 bar_g and a thermal input of up to 120 kW.

The BOOSTER test rig has a pneumatic dense-phase conveying system. It consists of a pressure vessel (1 m^3) mounted on weighing cells. Inside the vessel, a stirrer loosens the fuel and prevents bridging. At the bottom of the vessel, N_2 is introduced to form a fluidized bed. The fuel exits the vessel and is conveyed to the gasifier by an additional mass flow of N_2. The dosing pipe has an inner diameter of 6 mm. The fuel mass flow is directly proportional to the pressure difference between the dosing vessel and the gasifier. It is regulated by inflating or deflating the dosing vessel with N_2 according to the decrease in weight of the vessel measured by the weighing cells.

The gasifier consists of a cylindrical water-cooled pressure vessel. The reaction chamber inside the vessel has an inner diameter of 0.25 m and a length of 1.8 m (from the burner mouth to the end of the hot zone). It consists of a refractory lining with a high content of Al_2O_3 for a chemical resistance to slag and a thermal resistance up to 1800 °C. At the top of the chamber, a burner is mounted. The burner—especially designed for O_2 as a gasification agent—was used for the first time in this study The dosing pipe inserts the fuel directly without swirl centrically into a burner mouth. O_2 (preheated to 200 °C) is injected into the burner mouth with swirl through only one channel that surrounds the dosing pipe. In general, air instead of O_2 and the addition of H_2O and CO_2 are also possible with the BOOSTER test rig. Hot product gas is cooled down to 25 °C by water injection in the quench. A particle filter removes ash and coke particles from the product gas to prevent the pressure release valve and the downstream pipes from plugging. The product gas is finally combusted in a flare with a natural-gas pilot burner. Within the refractory lining, electrical heaters with an overall maximum electrical power of 32 kW are installed in the area from T1 to T5 (1.6 m). With these heaters, the inner wall of the reaction chamber can be heated up to ∼900 °C and kept warm during the entire test campaign. In order to increase the temperature to the expected temperature for the planned operation conditions, the burner can also be run on natural gas. No separate pilot burner is needed to start the gasification process. The fuel self-ignites after entering the reaction chamber and getting into contact with the gasification agent. Due to the cooling jacket of the pressure vessel and the relative large surface area in relation to the thermal input, heat losses are quite high. For an exemplary trial with disabled electrical heaters with RL at λ = 0.5 and a steam addition of 0.2 kg/kg_{fuel} (not part of the presented study), thermal losses around the reaction chamber are 11.6% of the total thermal input (fuel input based on LHV and gas preheating). These losses include losses to cooling water in the part of the pressure vessel surrounding the reaction chamber, the gasifier top and cam (all measured), as well as axial losses through the wall isolation to the cold quench and losses by radiation of the flame to the quench (both estimated by calculations). The same operation point was carried out with enabled electrical heaters in the wall. The absolute measured/calculated losses were higher with heaters, but after subtracting the power of the electrical heaters from the losses, the actual losses the reaction chamber and the flame could see were 8.2%. Hence, the electrical heaters lower the actual thermal losses. For commercial large-scale EFG plants, heat losses of ∼1−3% are assumed depending on the thermal input.[8] To keep the heat losses

DOI: 10.1021/acs.energyfuels.6b02949
Energy Fuels XXXX, XXX, XXX−XXX

Table 1. Calibrated Tar Compounds and Their Classifications

class	compound name					
2	phenol	cresol (o)	cresol (m)			
3	toluene	xylene (o)	styrene			
4	indene	naphthalene	biphenyl	fluorene	anthracene	phenanthrene
5	fluoranthene	pyrene	perylene			

as close as possible to these values, the electrical heaters are turned on during all presented trials. Actual thermal losses of the reaction chamber are between ~5% (for $\lambda = 0.35$) and ~12% ($\lambda = 0.55$) in this study. The design and engineering of the BOOSTER test rig has already been described in more detail.[42−44] Results of the gasification of HTC biomasses using the BOOSTER test rig and air as a gasification agent have already been published by Briesemeister et al.[45]

In this study, the gasifier gauge pressure was held constant at 0.2 bar_g, and the thermal input based on lower heating value (LHV) was maintained at ~70 kW. The main operation parameter investigated in this study was the oxygen stoichiometric ratio λ as defined in eq 11, where $\dot{m}_{O_2,min}$ is the minimum O_2 mass flow needed for complete stoichiometric combustion and $\dot{m}_{O_2}$ is the actual injected O_2 mass flow. In order to keep λ constant, even though fuel input fluctuates slightly, the required O_2 mass flow was calculated online and was regulated by a mass flow controller. In this study, λ was varied between 0.35 and 0.55.

$$\lambda = \frac{\dot{m}_{O_2}}{\dot{m}_{O_2,min}} \tag{11}$$

3.2. Measurement Methods and Calculations. *Temperature.* For temperature measurements, six thermocouples of type R (T1−T6) were installed in the refractory lining along the height of the reaction chamber (Figure 1). The tips of the thermocouples end at the inner wall of the chamber.

Particle Sampling. Particles were taken with a sampling probe (oil tempered at 150 °C) from the end of the reaction chamber before passing the quench and were collected in a sinter metal filter. Soot and char were not separated in this study. Carbon conversion and overall fuel conversion were calculated using the ash tracer method taking into account all ash compounds. Its widely used in literature for coal as well as for biomass to calculate conversion rates without knowing the absolute weight loss of the fuel during conversion.[31,46−50] The assumption of the ash tracer method is that the mass of the ash in the fuel does not change during gasification. By determining ash contents and elemental compositions, the carbon conversion (C_c) and overall fuel conversion (C_{ov}) can be calculated using eqs 12 and 13, where x_0 and x are the weight contents (on a dry base (db)) in the fuel and the sampled char probes, respectively. Derivations of eqs 12 and 13 are presented in detail by Tremel.[31]

$$C_C = 1 - \frac{x_C \cdot x_{0Ash}}{x_{0C} \cdot x_{Ash}} \tag{12}$$

$$C_{ov} = \frac{1 - \frac{x_{0Ash}}{x_{Ash}}}{1 - x_{0Ash}} \tag{13}$$

Gas Analysis. The composition of the dry gas (CO, CO_2, CH_4, H_2, O_2) was measured online using a Sick S700 module with infrared spectroscopy, thermal conductivity detector, and a paramagnetic O_2 sensor. The N_2 content was calculated by taking the difference to 100%. For the measurement of the water content in the product gas, a capacitive humidity sensor was installed. LHV_{pg} of the product gas (in kJ/Nm^3) was calculated from the measured contents of CO, H_2, and CH_4.

Cold Gas Efficiency (CGE). CGE is defined as the ratio of the chemical power of the product gas to the chemical power of the fuel feed (eq 14).

$$CGE = \frac{\dot{V}_{pg} \cdot LHV_{pg}}{\dot{m}_{fuel} \cdot LHV_{fuel}} \tag{14}$$

$\dot{m}_{fuel}$ is the fuel mass flow in kilogram per hour, and LHV_{fuel} is the lower heating value of the fuel in kilojoules per kilogram. Product gas volume flow rate $\dot{V}_{pg}$ cannot be measured directly. It is calculated using eq 15 under the assumption that all of the converted carbon—as measured by the ash tracer method—remains in the product gas as CH_4, CO, or CO_2. V_{mol} is the molar gas volume, and M_c is the molar mass of carbon. y_i is the molar content of CH_4, CO, and CO_2 in the product gas. In this case, x_{0C} is on an "as received" (ar) basis.

$$\dot{V}_{pg} = \frac{C_C \cdot x_{0C(ar)} \cdot V_{mol} \cdot \dot{m}_{fuel}}{M_C \cdot (y_{CH_4} + y_{CO} + y_{CO_2})} \tag{15}$$

SPA Sampling. Tar sampling was carried out using a hot probe (heated to 300 °C) located at the end of the reaction chamber. The applied method is based on solid-phase adsorption (SPA).[37] Analysis of the SPA samples was done by a quantitative method using gas chromatography with a flame ionization detector (Agilent 7890A). Calibrated tars and their classification[41] are shown in Table 1. For a rough estimation of the amount of noncalibrated yet detected tars ("unknowns"), an average calibration factor was used.

All of the values based on gas analysis or temperatures shown in the present work are arithmetic averages over at least 10 min of stable operation (stable temperature, gas analysis and flame). SPA and particle samplings were also carried out during stable operations.

3.3. Fuels. In this study, four biomasses and one lignite were investigated:

Torrefied wood (TW) is an industrial product delivered in pellet form. Milling was carried out externally in a two stage process (cutting mill and ball mill) with subsequent sieving with a 250 μm mesh. TW originates from a mixture of deciduous and coniferous wood (according EN 14961-1 type 1.1.). TF was carried out at 290 °C for 45 min. According to a declaration of the manufacturer (JRS Rettenmaier), the treatment of the raw biomasses *beech wood* (B; product code: HB 120) and *corn cobs* (CoC; product code: MK 100) consisted only of drying, grinding, and sieving. CoC is a residual of corn harvesting and was not used energetically until now. *Hydrothermal carbonized green waste (HCG)* was produced in a HTC demonstration plant at 210 °C with a residence time of 3 h and a pressure of 20−21 bar. The feedstock was washed before it entered the HTC plant. After carbonization, mechanical dewatering, thermal drying, and milling were carried out. *Rhenish lignite (RL)* was purchased directly from the manufacturer as a filter dust. No further treatment was necessary. Table 2 illustrates the chemical and physical properties of the fuels. All measurements were carried out in the institute's own laboratory according to the following standard industrial methods: ultimate analysis DIN 51732 and DIN 51717; heating value DIN 51900-1; proximate analysis DIN 51718, DIN 1720, DIN 51719 (for RL), and DIN EN 14775 (for TW, B, and HCG). CoC was ashed at 450 °C instead of 550 °C because a sintering already occurred at 550 °C.

The fuel properties can be described in a Van Krevelen diagram (Figure 2). The raw biomasses B and CoC have the highest O/C and H/C ratios. Due to the release of H_2 and O_2 during the thermal pretreatment, the ratios for TW and HCG are lower, and the level of carbonization is increased, more toward that of coal. HCG lies in the area of lignite, and TW still lies in the range of peat. LHV_{fuel} increases in the order CoC < B < TW < RL < HCG. The slightly lower LHV of RL compared to HCG originates from the lower moisture content of HCG.

The fuels also differ in particle size and particle size distribution (Table 2). Particle sizes and shapes can be observed in the optical

DOI: 10.1021/acs.energyfuels.6b02949
Energy Fuels XXXX, XXX, XXX−XXX

Table 2. Chemical and Physical Properties of the Fuels, All Values on an "As Received" (ar) Basis

	torr. wood (TW)	beech (B)	HTC green waste (HCG)	corn cobs (CoC)	rh. lignite (RL)
ultimate analysis in wt %					
C	53.1	48.2	59.8	44.7	60.3
H	5.2	5.2	5.2	5.4	5.5
N	0.6	0.3	0.7	0.3	0.7
S	0.3	0.3	0.3	0.1	0.5
O (calculated)	31.7	38.3	26.7	39.7	17.5
Cl	0.017	0.008	0.042	0.19	0.041
proximate analysis in wt %					
moisture	5.5	6.4	2.3	8.4	13.3
ash	3.6	1.1	4.9	1.3	3.92
volatile yield	64.8	78.9	59.7	73.5	46.2
fixed carbon	26.2	13.7	33.1	16.9	36.6
lower heating value (kJ/kg)					
LHV_{fuel}	19724	17311	22747	16292	22709
particle size analysis (μm)					
d_{10}	25	28	7	133	15
d_{50}	103	124	57	221	57
d_{90}	224	263	175	371	168
bulk density (kg/m^3)					
ρ_{bulk}	468	327	485	416	616

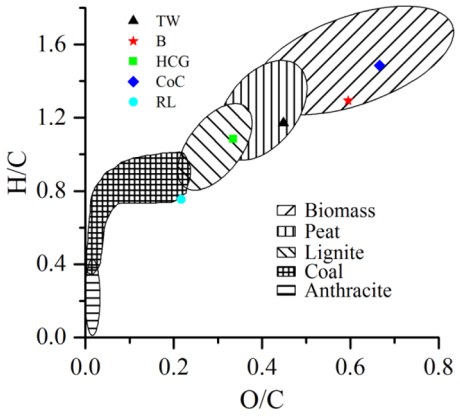

Figure 2. Fuels plotted in a Van Krevelen diagram.

microscope pictures of the fuels (Figure 3). The particles of B and CoC are significantly larger than the particles of the other fuels. Due to the fact that a thermally untreated biomass has a higher volatile matter content and a higher reactivity, the particle sizes of B and CoC are still expected to be sufficient for high conversion rates. Hence, no further grinding is necessary. B shows a fiber-like structure, whereas particles of CoC have a smooth surface. The darker colors of TW and HCG compared to the raw biomasses is in line with the higher degree of carbonization compared to the raw biomasses illustrated in the Van Krevelen diagram (Figure 2).

4. RESULTS AND DISCUSSION

Table 3 lists the actual values for all trials: λ (including error calculations), thermal inputs P_{fuel}, the feeding rates $\dot{m}_{fuel}$ and $\dot{m}_{O_2}$, as well as the actual N_2 input by fuel dosing $\dot{m}_{N_2\_dosing}$. The estimated plug flow residence time τ in the hot zone—based on the average temperature (T1 to T5) and all input flow rates—is also presented in Table 3. Real particle residence time is expected to be significantly lower since the increasing gas volume is not taken into account for calculation of τ. Due to the lower LHV_{fuel} of the raw biomasses B and CoC, the fuel feeding rate was higher in order to reach the same thermal input. Therefore, for the following interpretation of the results, the absolute input of all fuel components in kilograms per hour, not only the mass percentage of the fuel (Table 3), has to be taken into account.

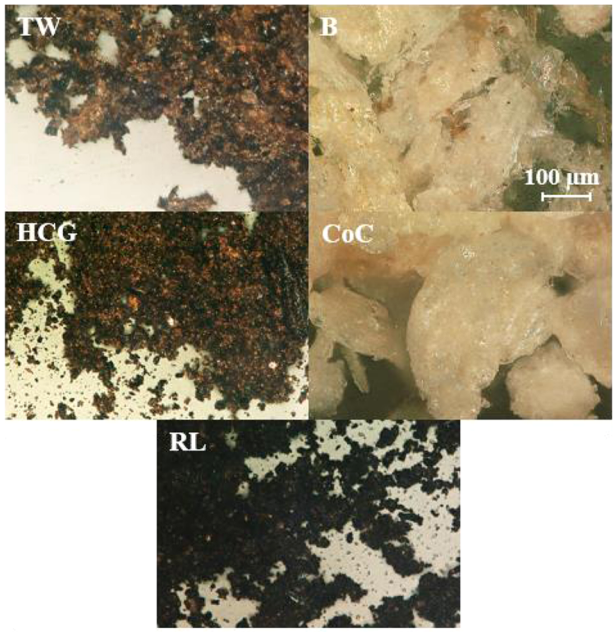

Figure 3. Optical microscope pictures of the fuels.

Table 3. Summary of Performed Trials

fuel	λ	P_{fuel} kW	$\dot{m}_{fuel}$ kg/h	$\dot{m}_{O2}$ kg/h	$\dot{m}_{N2\_dosing}$ kg/h	τ s
TW	0.350 ± 0.009	69.9	12.8	6.8	1.1	10.3
	0.400 ± 0.010	71.1	13.0	7.9	0.9	9.2
	0.450 ± 0.011	72.8	13.3	9.1	1.1	8.1
	0.500 ± 0.013	71.3	13.0	9.9	1.0	7.7
	0.550 ± 0.014	70.0	12.8	10.7	0.8	7.2
B	0.361 ± 0.009	69.9	14.5	6.9	1.6	9.6
	0.416 ± 0.011	69.1	14.4	7.9	1.7	8.5
	0.468 ± 0.012	70.1	14.6	9.0	1.7	7.3
	0.521 ± 0.013	69.6	14.5	10.0	1.6	6.8
	0.572 ± 0.014	67.9	14.1	10.7	1.7	6.2
HCG	0.350 ± 0.009	76.0	12.0	7.4	1.2	9.7
	0.40 0 ± 0.010	77.2	12.2	8.6	1.3	8.5
	0.450 ± 0.011	74.8	11.8	9.4	1.3	7.7
	0.500 ± 0.013	72.5	11.5	10.1	1.5	6.8
	0.550 ± 0.014	75.8	12.0	11.6	1.4	6.0
CoC	0.350 ± 0.009	71.6	15.8	6.9	0.9	10.6
	0.400 ± 0.010	73.0	16.1	8.0	0.9	9.5
	0.450 ± 0.011	73.1	16.2	9.0	0.9	8.3
	0.500 ± 0.013	72.9	16.1	10.0	0.9	7.3
	0.550 ± 0.014	72.6	16.0	11.0	1.0	6.6
RL	0.339 ± 0.009	74.8	11.9	7.0	0.8	10.9
	0.400 ± 0.010	75.9	12.0	8.4	1.1	9.2
	0.450 ± 0.011	74.0	11.7	9.2	1.1	8.5
	0.500 ± 0.013	63.8	10.1	8.8	0.8	8.8
	0.550 ± 0.014	75.8	12.0	11.5	0.8	6.7

4.1. Fuel Feeding Behavior. Fuel feeding behavior depends on the physical properties of the fuel (particle size, shape, and density). In order to increase overall plant efficiency,

DOI: 10.1021/acs.energyfuels.6b02949
Energy Fuels XXXX, XXX, XXX−XXX

the inert gas demand for fluidization and pneumatic feeding (additional carrier gas) has to be as low as possible. The optimum amount of fluidizing gas is defined as the lowest gas demand for which a stable and continuous flow of fuel out of the pressure vessel of the dosing system is guaranteed. Additional carrier gas is at its optimum at the lowest gas demand before plugging occurs and the flame in the gasifier becomes unstable and starts fluctuating. An unstable flame due to discontinuous fuel feeding leads to a poor gas quality. Fuel loading in the conveying pipe (fuel in kg/gas in kg) depends on the two above-mentioned gas flow rates, mainly, however, on the additional carrier gas. Absolute values are plant specific. To get a general idea of the feeding behavior, they are normalized to the values obtained with Rhenish lignite (RL; Figure 4).

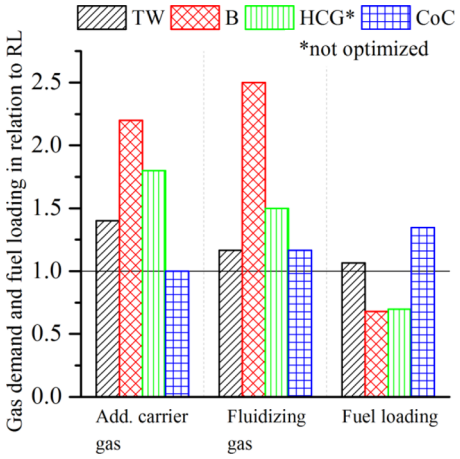

Figure 4. Gas demand and fuel loading in the conveying pipe for each biomass in relation to RL for the same thermal input (average values of the trials).

For TW, the fuel loading laid in the range obtained with RL. The gas consumption was slightly higher, but a further optimization—especially of the additional carrier gas—seems possible since nearly no feeding problems were observed. HCG was one of the first fuels investigated with the BOOSTER test rig. Therefore, the focus was more on a stable plant operation. As a result, an optimization of the gas demand was not carried out. The high values led to a lower fuel loading compared to RL. Due to the very similar physical properties (Table 2, Figure 3) and the fact that no feeding problems were observed during trials, it can be expected that the same values as those obtained with RL can be reached with HCG. A completely different behavior was shown by B and CoC, although they are both raw biomasses. The gas demand for B—both additional carrier and fluidizing gas—was more than twice that needed for RL. This led to a poor fuel loading and therefore to a high dilution of the product gas with N_2. Despite the high amounts of gas needed, frequent plugging occurred at the vessel outlet as well as in the conveying pipe. Besides that, the fuel tended to build bridges in the dosing vessel, requiring a usage of the stirrer, which could solve the problem. The particle size compared to TW is not significantly different (Table 2). Hence, the fiber-like structure of raw beech wood particles is assumed to be the reason for this behavior. As shown in Figure 3, the particles of B are more conglutinated with its fibers, whereas the CoC particles are more separated due to their smooth surface. The poor pneumatic feeding behavior of the raw wood powder corresponds to the results of van der Drift et al.[14] Pipe plugging in a large industrial plant is expected to be a minor problem due to the larger pipe diameters. However, due to the high amounts of gas needed and the dilution of the product gas, a pneumatic feeding system for this type of fuel seems difficult to handle. In contrast, CoC exhibit very good feeding behavior. Gas amounts were in the range of RL, and the fuel loading was even higher. In spite of its large particle size compared to that of other fuels, CoC seems to be suitable for pneumatic dense-phase feeding.

It can be concluded that the fuel feeding behavior depends not only on the particle size and the pretreatment but also on the feedstock and the shape of the particle. The following order from poor to good feeding properties was the result for the investigated fuels: B ≪ RL ≈ TW (≈ HCG) < CoC.

4.2. Temperature. Figure 5 illustrates the characteristic temperature profile of the reaction chamber wall from top (T1) to bottom (T6) for the different fuels. Data are not available for all of the operation points for T1 and T2. The temperatures were the highest at the top of the chamber where partial combustion occurs (reactions 1−5) and decreased subse-

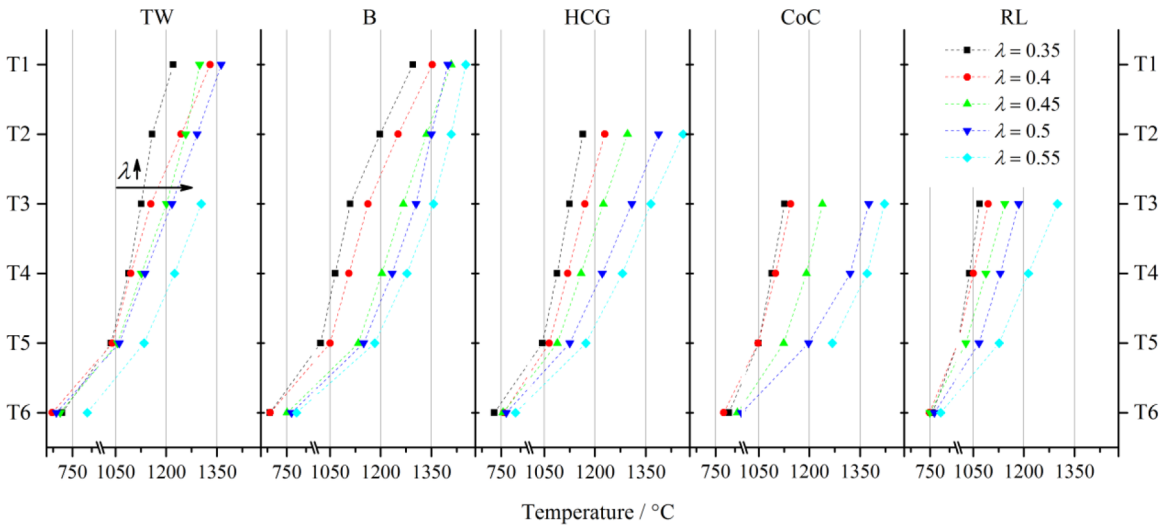

Figure 5. Axial temperature profiles inside the reactor for each fuel and varying λ (position of the thermocouples T1−T6 shown in Figure 1).

DOI: 10.1021/acs.energyfuels.6b02949
Energy Fuels XXXX, XXX, XXX−XXX

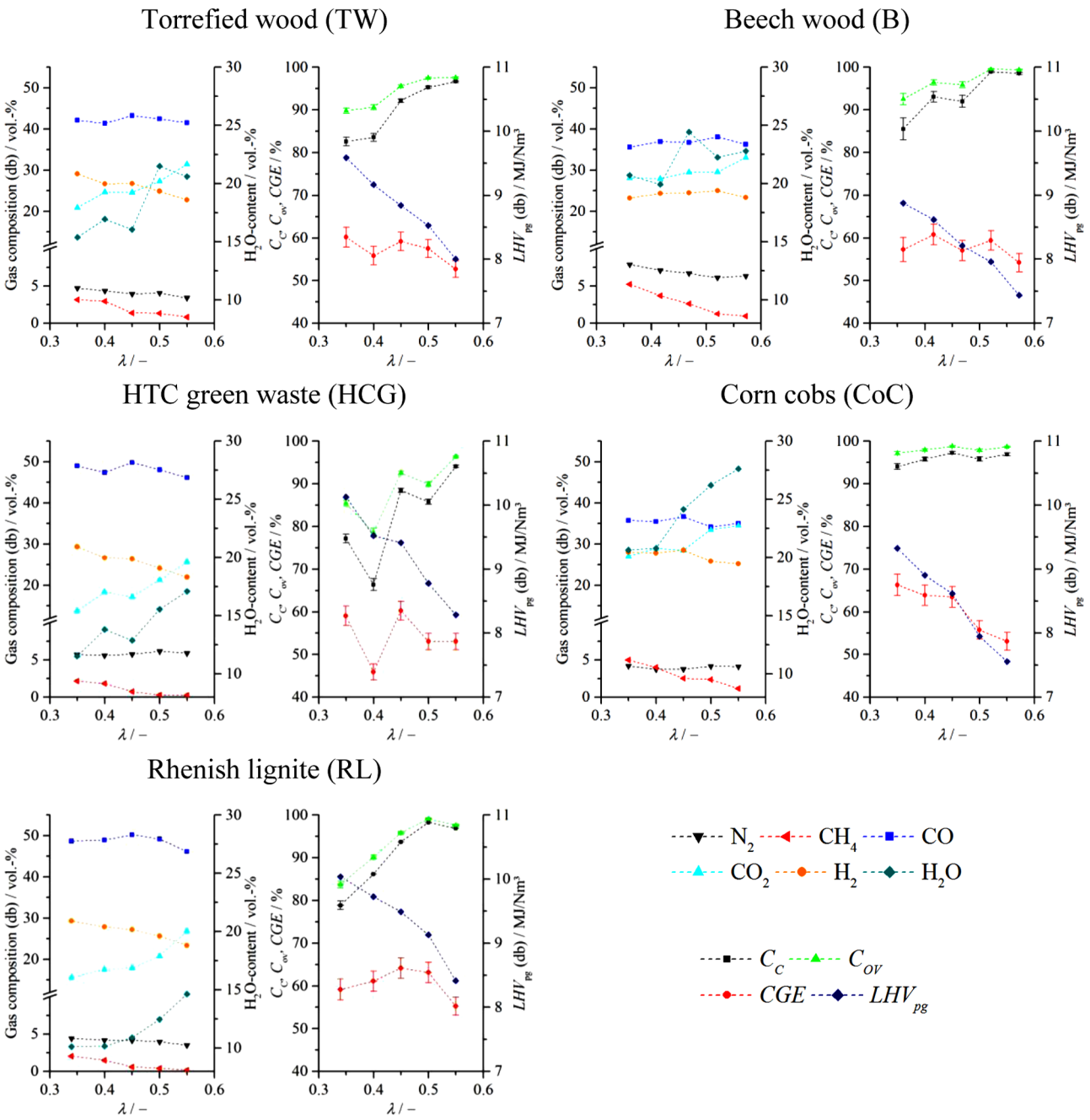

Figure 6. Conversion, cold gas efficiency, gas composition, and LHV of the product gas for each fuel.

quently due to heterogeneous gasification reactions 6–8 and thermal heat losses.

T6 showed a significant temperature drop in all trials and laid in the range between 640 and 870 °C. The influence of the cold water quench in this part of the chamber is strong. In addition, there is no electrical heating to compensate thermal losses in this part of the reaction chamber.

In general, temperatures clearly rose with increasing values of λ (the main parameter to control the temperature). TW and RL exhibited similar temperatures at high λ; at low λ, TW reached higher temperatures than RL. For HCG, which has fuel properties comparable to RL but a very low moisture content, the temperatures were higher than for RL for each λ. For λ = 0.5 and 0.55, CoC led to significantly higher temperatures than with HCG, although the moisture input of CoC trials was 4 times higher. A comparison of the temperatures during the TW and B trials in the upper zone (T1 and T2) of the chamber shows higher values for B. Hence, it can be concluded that not only λ but also the fuel parameters and the resulting product gas compositions have an effect on the temperature. To obtain a better understanding of the real temperature profile of the gas, suction pyrometer investigations will be done in future studies using five ports distributed over the height of the reaction chamber.

For further consideration, the process temperature *T3* is used because it is measured in the middle of the hot zone.

4.3. Conversion, Cold Gas Efficiency, and Gas Composition. Figure 6 illustrates the conversion (C_C and C_{ov}), CGE, gas composition, and LHV of the product gas for each fuel as a function of λ. An error calculation was done

DOI: 10.1021/acs.energyfuels.6b02949
Energy Fuels XXXX, XXX, XXX−XXX

separately for each trial and is included for the main performance parameters (C_C, C_{ov}, CGE). All denoted gas compositions were recalculated without N_2 purge gases from the flame detector and the camera (~1.5 N m^3/h). The real measured N_2-content given exemplarily for RL trials is 11−14% (db).

A typical curve progression can best be explained for RL: at λ = 0.35, C_C is low. At low temperatures, the char gasification reactions 6 and 7 are kinetically limited so that higher conversion rates in the short residence times of a few seconds cannot be reached. C_{ov} is always higher than C_C because all of the fuel compounds are taken into consideration. However, they converge at high conversion rates. C_{ov} almost reached a maximum (98.9%) for λ = 0.5. The slight decrease at λ = 0.55 is not plausible and can only be explained by errors in particle sampling or analysis. At increasing values of λ, the combustion reactions gain more influence. Therefore, CO_2 and H_2O increased, whereas H_2 decreased with an increase of λ. In contrast to H_2, CO did not decrease until λ = 0.45 because the additional gas volume provided by the risen conversion rate of the char with increasing λ consists mainly of CO (reactions 6, 7). Furthermore, the increasing temperatures due to an increase of λ favor the existence of CO by the homogeneous gas phase reactions 9 and 10. In the case of λ > 0.45, combustion reactions seemed to be predominant. CO is also oxidized so that the content of CO_2 and H_2O increased significantly. The increasing gas volume caused by higher conversions at higher λ values led to a decrease in percentage of N_2. CH_4 is <1 vol % for $\lambda \geq$ 0.45. The CH_4 seems to be a residual from devolatilization that is not completely decomposed or oxidized. Considering only a thermodynamic equilibrium, the formation of CH_4 according to eq 10 cannot occur at such high process temperatures. The presence of CH_4 in the product gas corresponds to the results of Dufour et al.,[51] who showed that the conversion of CH_4 in a syngas is kinetically limited also at high temperatures (1300 °C). The above-mentioned evolution of the gas composition leads to decreasing LHV_{pg}. An optimum value for CGE is obtained when high conversion rates and high values of LHV_{pg} are reached at the same time. In this case, the highest value of CGE was 64.2% at λ = 0.45.

Already at low values of λ, the raw biomasses CoC and B exhibit values of C_{ov} > 90%. For CoC, C_{ov} is 97% at λ = 0.35. A significant increase in conversion is not possible by increasing the value of λ, and therefore the volume of gas produced is also not increased. This is why the highest CGE of CoC—which is also the highest CGE of all trials—was determined at λ = 0.35 and reached 66.3%. The CH_4 ratio is quite high for low values of λ—still reaching 1.1 vol % at λ = 0.55. The same behavior was also observed for B and corresponds to the results of Weiland et al.[12] Due to the high content of volatile matter in the raw biomass, a high amount of CH_4 and other pyrolysis gases were produced during devolatilization. Due to the large uncertainty in the value of CGE of B, it is not possible to determine an explicit optimum. However, taking into consideration the conversion rates, λ has to be higher than for CoC.

For the two thermally pretreated biomasses TW and HCG, a higher value of λ than for the raw biomasses was needed to reach adequate conversion rates. The significant drop in conversion for HCG at λ = 0.4 cannot be explained and may be due to errors in particle sampling. For HCG, the share of CO, H_2, CO_2, and CH_4 is very similar to that of RL. For TW, the percentage of CH_4 is clearly lower (0.8 vol % at λ = 0.55). As in the case for B, the operation point with the highest value for CGE could not be clearly determined. However, taking into account the conversion rates, λ = 0.45 seems to be reasonable.

N_2 content in the product gas was highest for B followed by HCG due to the low fuel loading. For CoC, the effect of higher fuel loading on N_2 dilution is compensated by the higher demand of fuel to reach the same thermal input. Hence, the percentage of N_2 in the CoC trials was in the same range as for TW and RL.

The theoretical temperature of the thermodynamic equilibrium of the water gas shift, reaction 9, was calculated from the measured gas composition. It was found to be between 870 and 1040 °C. Due to the inaccurate measurement of H_2O, the calculated values can only be a rough estimation. HCG exhibits a high equilibrium temperature (1005−1030 °C) in all trials, whereas RL and CoC generally exhibit low equilibrium temperatures (870−960 °C). B shows an intermediate behavior. The variations for TW are too high to give a general conclusion. Considering the temperature profiles (Figure 5), the calculated equilibrium temperature corresponds to the axial reactor temperature between the thermocouples T5 and T6. This suggests that homogeneous gas phase reactions do not take place toward the end of the reaction chamber.

The reactivity of all applied fuels is high enough to reach almost full conversion in the BOOSTER test rig. Due to the high conversion rates of CoC even at low values of λ, it seems to exhibit the highest reactivity of all investigated fuels.

The maximum CGE observed was 66.3%, which is quite low. For commercial-scale dry feed coal gasification plants, values up to 82% have been reported.[7] This is also the case for the two-stage Carbo-V biomass gasification process (CHOREN).[52] The low value of CGE in the present work can be attributed to the high heat losses that occur due to the water cooling. A commercial plant will not have a water-cooled pressure vessel, and furthermore heat losses are not proportional to the thermal input. Weiland reports a CGE of 57−76% for a similar EFG test rig (PEBG). A total of 76% was reached with a thermal input of 600 kW using stem wood powder.[53]

The LHV_{pg} laid between 7.4 and 10.3 MJ/Nm^3 for all of the trials, which is in the range reported in the literature for autothermal biomass gasification with O_2 as a gasification agent (6−11 MJ/Nm^3[54]). The LHV_{pg} of the raw biomasses B and CoC is generally slightly lower than the LHV_{pg} of the pretreated biomasses TW and HCG as well as of RL. For all fuels, the product gas could be used for power generation by direct combustion. In this case, all combustible compounds are completely used, and it is not necessary to lower the content of CH_4.

Due to the quite low dilution of N_2 in the product gas, it is suitable for the production of liquid synthetic fuels in processes such as the Fischer−Tropsch (FTS) or methanol syntheses. Since only CO and H_2 are converted in these processes, it is important to lower the CH_4 content as far as possible. A H_2/CO ratio of 1.7 in the product gas is required for the low temperature FTS process, whereas a 2.6 ratio is needed for the high temperature FTS process.[7] For all trials, the ratio was between 0.5 and 0.78. The ratio was highest for CoC (0.72−0.78). In general, the H_2/CO ratio decreased with increasing values of λ. This behavior was also observed by Weiland et al.[12] It can be adjusted by the addition of steam as the amount of H_2 increases as a result according to eq 9. However, a water−gas shift reactor will be needed to reach the required ratio for FTS.

DOI: 10.1021/acs.energyfuels.6b02949
Energy Fuels XXXX, XXX, XXX−XXX

4.4. Tars. For a utilization of the product gas in combustion processes or syntheses, a knowledge of the tar content and the tar dew point is necessary. Therefore, Figure 7 illustrates the

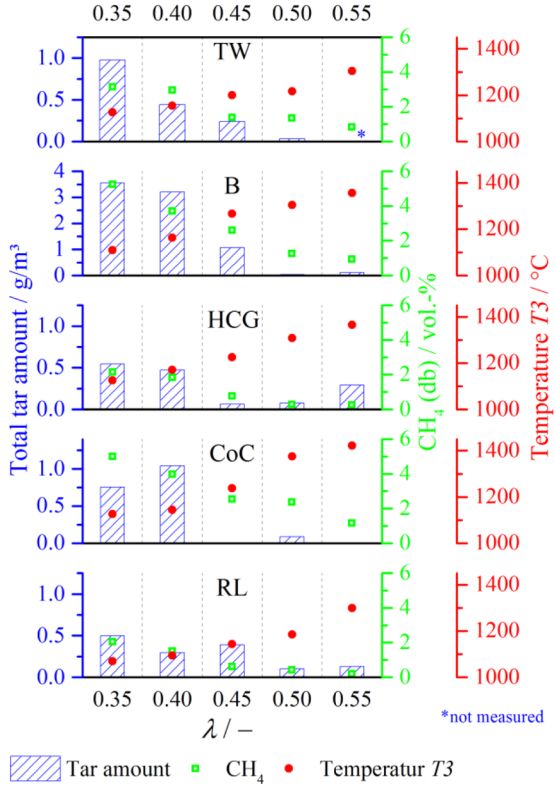

Figure 7. Influence of λ on total tar amount, volume percentage CH_4, and process temperature T3.

influence of λ on the total tar amount (sum of all identified tars + unknowns), the CH_4 content of the product gas, and the process temperature (T3) for all fuels. Tars were detected for all fuels, although the process temperature T3 was >1050 °C. The evolution of the amount of tar corresponds to that of CH_4, which decreases with increasing temperatures. The tar amount for B was significantly higher than for all other fuels. A total of 3.5 g/m^3 was measured at λ = 0.35. At λ = 0.45, it was still >1 g/m^3. For all other fuels including CoC, the total tar amount was <1g/m^3 at all operation points. The comparable high value for HCG at λ = 0.55 seems not logical and cannot be explained. Further investigations are needed. The high tar amounts for B at low values of λ can be explained by the feedstock characteristics. B as a raw, thermally untreated woody biomass is expected to have the strongest lignin content of all investigated fuels. Therefore, the high tar amounts measured for B at low λ values correspond to the results of Yu et al.,[38] who measured more stable tars from decomposition of lignin than from cellulose and hemicellulose. TW exhibited a significantly lower tar amount, although the feedstock was similar. The influence of TF on the decomposition mechanisms of biomass has already been described in the literature.[11,25,27] Light volatiles are released, and lignin is thermally softened and partially devolatilized during TF. Hence, TF can lead to lower tar amounts compared to the raw biomass.[55,56] This seems to be the case for TW.

In order to draw conclusions from the formation of tar, Figure 8 illustrates the tar composition and the amount of every

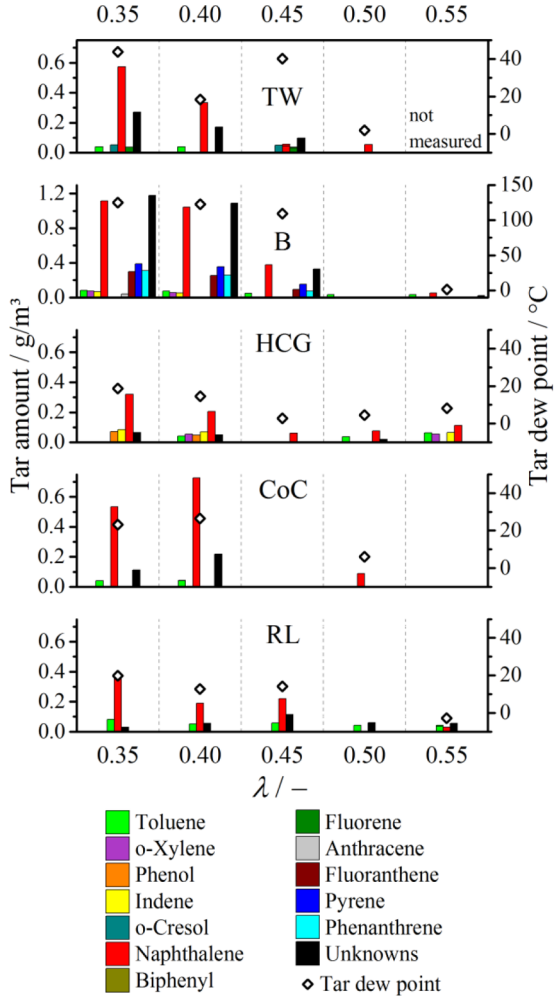

Figure 8. Influence of λ on detailed tar composition and tar dew point.

single identified compound. The individual concentrations are needed to calculate the tar dew points using the ECN tar dew point calculator.[41] Tar dew points are also shown in Figure 8 (as far as predictable).

Mainly toluene and naphthalene were detected for TW, CoC, and RL. According to the classification of Milne et al.,[39] these are tertiary tars. For HCG, some additional compounds were detected, o-xylene and phenol, representing secondary tars, and indene, representing a tertiary tar. The amount of all compounds except naphthalene was <0.1 g/m^3 for HCG. Pyrene, phenanthrene, and fluoranthene—all tertiary tars—were detected for B. As expected at high temperatures, no primary devolatilization products were detected. The measured tars were all generated by the recombination of decomposed devolatilization products.

According to the tar composition and the high tar amount for B at λ = 0.35 to λ = 0.45, the calculated tar dew point in these cases is the highest of all trials (110−125 °C). For TW, tar dew point reaches up to 44 °C, whereas for all other fuels it lies between 0 and 25 °C. For the direct utilization of the product gas in a combustion process (e.g., gas turbine), it is necessary to keep the temperature always above the tar dew point. This seems possible for all of the tested fuels and operation points without any additional gas treatment for the tars. For synthesis processes such as the Fischer−Tropsch process or methanol syntheses, the focus lies on decreasing the

DOI: 10.1021/acs.energyfuels.6b02949
Energy Fuels XXXX, XXX, XXX−XXX

CH_4 content, which can be achieved by operating at higher values of λ, additionally leading to lower tar amounts. However, due to the fact that for synthesis processes even an amount of a few milligrams per cubic meter is a problem, tar treatment of the product gas could be necessary anyway.

5. CONCLUSION AND OUTLOOK

Four different biomasses were investigated with regard to their applicability in an oxygen-blown entrained flow gasifier equipped with a dense-phase pneumatic feeding system. The results were compared with Rhenish lignite. In general, the feasibility was confirmed.

Corn cobs (CoC) exhibited the best feeding behavior with the highest fuel loading, although their particle size is the largest of all investigated fuels. Beech wood powder (B) does not seem suitable for stable long-term operation of an EFG with a pneumatic dense-phase feeding system. Due to its fiber-like structure, a high amount of carrier gas was necessary and pipe plugging occurred. All other fuels are appropriate for a long-term operation with this feeding system.

All fuels exhibited a good conversion. For B and CoC, a lower λ than for the other fuels is sufficient to achieve high conversion rates. The best CGE was reached using CoC at a low λ of only 0.35. Both CoC and B generated high amounts of CH_4. In order to reduce CH_4 to <1 vol % for CoC, B, and torrefied wood (TW), a λ of at least 0.55 was needed. Regarding feeding behavior, conversion rates and gas composition HCG as well as TW seems generally suitable as a substitute in coal fed gasification plants. To the best of author's knowledge, no publications about the use of hydrothermal carbonized biomass in an oxygen-blown EFG have been available until now. The EFG of HCG needs further investigation since the quite low conversion rate at λ = 0.4 and the comparatively high tar amount at λ = 0.55 seem not to be logical.

EFG is often considered to be a tar-free technology, although comprehensive studies about tar amount and tar composition in the hot product gas of a biomass fed EFG are rare. In this study, tars were detected for all fuels especially at low λ values. By far, the highest amount of tar in the product gas was measured for B. A total of 3.5 g/m^3 was detected at λ = 0.35, mainly consisting of tertiary tars (e.g., naphthalene). This suggests that tar was formed by a recombination of decomposed devolatilization products. Depending on the operation condition, the fuel type, and the product gas utilization, the presented study shows that a tar treatment of the product gas of a biomass fed EFG could be necessary.

Ash and slagging behavior were not taken into account in this study. Since a knowledge of this issue is important for a stable, long-term operation, it will be investigated in future work.

Fuel loading in the conveying pipe can be significantly increased in an industrial-scale plant due to the larger pipe diameters. Therefore, the specific N_2 demand can be lowered. An N_2 content of <2 vol % in the product gas seems to be a realistic value. Besides, the CGE in an industrial plant is expected to be higher than the value achieved in this study since the ratio of thermal losses and fuel input is significantly lower.

AUTHOR INFORMATION

Corresponding Author

*E-mail: Michael.Kremling@tum.de.

ORCID

Michael Kremling: 0000-0002-8616-430X

Notes

The authors declare no competing financial interest.

ACKNOWLEDGMENTS

This work is part of the project "Thermal utilization of biomasses in high-temperature processes" (FKZ 220 239 11) funded by the German Federal Ministry for Agriculture and Food. The support of the TUM Graduate School is thankfully acknowledged.

ABBREVIATIONS

B = beech
C_C = carbon conversion
CGE = cold gas efficiency
CoC = corn cobs
C_{ov} = overall conversion
ECN = Energy Research Center of The Netherlands
EFG = entrained flow gasification
FBG = fluidized-bed gasification
FTS = Fischer−Tropsch synthesis
HCG = hydrothermal carbonized green waste
HTC = hydrothermal carbonization
LHV = lower heating value
TF = torrefaction
TW = torrefied wood
SPA = solid phase adsorption
RL = Rhenish lignite

REFERENCES

(1) *Energy Roadmap 2050*; European Commission: Luxembourg, 2012.
(2) *Paris Agreement*; United Nations Framework Convention on Climate Change: Paris, 2015.
(3) Kaltschmitt, M.; Hartmann, H.; Hofbauer, H. *Energie aus Biomasse*; Springer: Berlin, 2016.
(4) Ahrenfeldt, J.; Thomsen, T. P.; Henriksen, U.; Clausen, L. R. *Appl. Therm. Eng.* **2013**, *50*, 1407−1417.
(5) Alauddin, Z. A. B. Z.; Lahijani, P.; Mohammadi, M.; Mohamed, A. R. *Renewable Sustainable Energy Rev.* **2010**, *14*, 2852−2862.
(6) Spliethoff, H. *Power Generation from Solid Fuels*; Springer: Berlin, 2010.
(7) Higman, C.; van der Burgt, M. *Gasification*; Elsevier: Boston, 2008.
(8) Tremel, A.; Becherer, D.; Fendt, S.; Gaderer, M.; Spliethoff, H. *Energy Convers. Manage.* **2013**, *69*, 95−106.
(9) Swanson, R. M.; Platon, A.; Satrio, J. A.; Brown, R. C. *Fuel* **2010**, *89*, S11−S19.
(10) Weiland, F.; Hedman, H.; Marklund, M.; Wiinikka, H.; Öhrman, O.; Gebart, R. *Energy Fuels* **2013**, *27*, 932−941.
(11) Weiland, F.; Nordwaeger, M.; Olofsson, I.; Wiinikka, H.; Nordin, A. *Fuel Process. Technol.* **2014**, *125*, 51−58.
(12) Weiland, F.; Wiinikka, H.; Hedman, H.; Wennebro, J.; Pettersson, E.; Gebart, R. *Fuel* **2015**, *153*, 510−519.
(13) Öhrman, O. G.; Weiland, F.; Pettersson, E.; Johansson, A.-C.; Hedman, H.; Pedersen, M. *Fuel Process. Technol.* **2013**, *115*, 130−138.
(14) van der Drift, A.; Boerrigter, H.; Coda, B.; Cieplik, M. K.; Hemmes, K. *Entrained Flow Gasification of Biomass: Ash Behaviour, Feeding Issues, and System Analyses*; Technical Report ECN-C-04-039, Energy Research Center of the Netherlands: Petten, Netherlands, 2004.
(15) Bergman, P. C. A.; Boersma, A. R.; Kiel, J. H. A; Prins, M. J.; Ptasinski, K. J.; Janssen, F. J. J. G. *Torrefaction for Entrained-Flow*

DOI: 10.1021/acs.energyfuels.6b02949
Energy Fuels XXXX, XXX, XXX−XXX

Gasification of Biomass; Technical Report ECN-C-05-067, Energy Research Center of the Netherlands: Petten, Netherlands, 2005.
(16) Qin, K.; Lin, W.; Fæster, S.; Jensen, P. A.; Wu, H.; Jensen, A. D. *Energy Fuels* **2013**, *27*, 262−270.
(17) Qin, K.; Lin, W.; Jensen, P. A.; Jensen, A. D. *Fuel* **2012**, *93*, 589−600.
(18) Gräbner, M. *Industrial Coal Gasification Technologies Covering Baseline and High-Ash Coal*; Wiley-VCH: Weinheim, 2015.
(19) van der Stelt, M.; Gerhauser, H.; Kiel, J.; Ptasinski, K. *Biomass Bioenergy* **2011**, *35*, 3748−3762.
(20) Svoboda, K.; Pohořelý, M.; Hartman, M.; Martinec, J. *Fuel Process. Technol.* **2009**, *90*, 629−635.
(21) *Status Overview of Torrefaction Technologies*; Task 32 report, IEA Bioenergy: Enschede, Netherlands, 2012.
(22) Phanphanich, M.; Mani, S. *Bioresour. Technol.* **2011**, *102*, 1246−1253.
(23) Arias, B.; Pevida, C.; Fermoso, J.; Plaza, M. G.; Rubiera, F.; Pis, J. J. *Fuel Process. Technol.* **2008**, *89*, 169−175.
(24) Dahlquist, E. *Technologies for Converting Biomass to Useful Energy: Combustion, Gasification, Pyrolsis, Torrefaction and Fermentation*; CRC Press: Boca Raton, FL, 2013.
(25) Chew, J. J.; Doshi, V. *Renewable Sustainable Energy Rev.* **2011**, *15*, 4212−4222.
(26) Erlach, B.; Harder, B.; Tsatsaronis, G. *Energy* **2012**, *45*, 329−338.
(27) Pandey, A.; Bhaskar, T.; Stöcker, M.; Sukumaran, R. *Recent Advances in Thermochemical Conversion of Biomass*; Elsevier Science: Burlington, MA, 2015.
(28) Bach, Q.-V.; Skreiberg, Ø. *Renewable Sustainable Energy Rev.* **2016**, *54*, 665−677.
(29) Viguié, J.-C.; Ullrich, N.; Porot, P.; Bournay, L.; Hecquet, M.; Rousseau, J. *Oil Gas Sci. Technol.* **2013**, *68*, 935−946.
(30) Badeau, J.-P.; Levi, A. *Biomass Gasification: Chemistry, Processes, and Applications*; Nova Science Publishers: Hauppauge, NY, 2009.
(31) Tremel, A. *Reaction Kinetics of Solid Fuels during Entrained Flow Gasification*; Dr.-Hut: München, 2012.
(32) Tremel, A.; Spliethoff, H. *Fuel* **2013**, *103*, 663−671.
(33) Tremel, A.; Spliethoff, H. *Fuel* **2012**, *107*, 653−661.
(34) Tremel, A.; Spliethoff, H. *Fuel* **2013**, *107*, 170−182.
(35) Smoot, L. D. *Coal Combustion and Gasification*; Plenum Press: New York, 1985.
(36) *Biomassevergasung - Teer und Staub in Produktgasen - Probenahme und analytische Bestimmung*; (DIN CEN/TS 15439) Deutsches Institut für Normung: Berlin, 2006.
(37) Mayerhofer, M. *Teerentstehung und Teerminderung bei Allothermer Wirbelschichtvergasung*; Dr.-Hut: München, 2014.
(38) Yu, H.; Zhang, Z.; Li, Z.; Chen, D. *Fuel* **2014**, *118*, 250−256.
(39) Milne, T. A.; Evans, R. J.; Abatzaglou, N. *Biomass Gasifier "Tars": Their Nature, Formation, and Conversion*; National Renewable Energy Laboratory; Golden, CO, 1998.
(40) Rabou, L. P. L. M.; Zwart, R. W. R.; Vreugdenhil, B. J.; Bos, L. *Energy Fuels* **2009**, *23*, 6189−6198.
(41) Energy Research Center of the Netherlands. Thersites: The ECN tar dew point site. www.thersites.nl (accessed January 20, 2017).
(42) Kremling, M.; Briesemeister, L.; Spliethoff, H.; Gaderer, M. High-Temperature Biomass Gasification in an Entrained Flow Reactor—Design and Engineering of a Test Facility. *Proceedings of the 22st European Biomass Conference and Exhibition*, Hamburg, 2014.
(43) Kremling, M.; Briesemeister, L.; Fendt, S.; Gaderer, M.; Spliethoff, H. High temperature biomass gasification in an entrained flow reactor − Commissioning and first trials of a 100 kW test facility. *Proceedings of 2nd International Conference on Renewable Energy Gas Technology*, Barcelona, 2015.
(44) Kremling, M.; Briesemeister, L.; Fendt, S.; Gaderer, M.; Spliethoff, H. Oxygen-blown entrained flow gasification of biomass - results from a 100 kW test rig. *Proceedings of the 24st European Biomass Conference and Exhibition*, Amsterdam, 2016.
(45) Briesemeister, L.; Kremling, M.; Fendt, S.; Spliethoff, H. *Chem. Eng. Technol.* **2017**, *40*, 270.
(46) Botteghi, F. *Experimental Investigation of High- Pressure, High-Temperature Solid Fuel Gasification*; Dr.-Hut: München, 2015.
(47) Tchapda, A. H.; Pisupati, S. V. *Fuel* **2015**, *156*, 254−266.
(48) Li, J.; Bonvicini, G.; Biagini, E.; Yang, W.; Tognotti, L. *Fuel* **2015**, *143*, 492−498.
(49) Simone, M.; Biagini, E.; Galletti, C.; Tognotti, L. *Fuel* **2009**, *88*, 1818−1827.
(50) Yeasmin, H.; Mathews, J. F.; Ouyang, S. *Fuel* **1999**, *78*, 11−24.
(51) Dufour, A.; Valin, S.; Castelli, P.; Thiery, S.; Boissonnet, G.; Zoulalian, A.; Glaude, P.-A. *Ind. Eng. Chem. Res.* **2009**, *48*, 6564−6572.
(52) Althapp, A. Kraftstoffe aus Biomasse mit dem Carbo-V-Vergasungsverfahren. *FVS Fachtagung* 2003.
(53) Weiland, F. *Pressurized Entrained Flow Gasification of Pulverized Biomass*; Luleå University of Technology: Luleå, 2015.
(54) Karl, J. *Dezentrale Energiesysteme: Neue Technologien im Liberalisierten Energiemarkt*; Oldenbourg; München, 2012.
(55) Dudyński, M.; van Dyk, J. C.; Kwiatkowski, K.; Sosnowska, M. *Fuel Process. Technol.* **2015**, *131*, 203−212.
(56) Raut, M. K.; Basu, P.; Acharya, B. *International Journal of Renewable Energy & Biofuels* **2016**, *2016*, No. 823723.

DOI: 10.1021/acs.energyfuels.6b02949
Energy Fuels XXXX, XXX, XXX−XXX